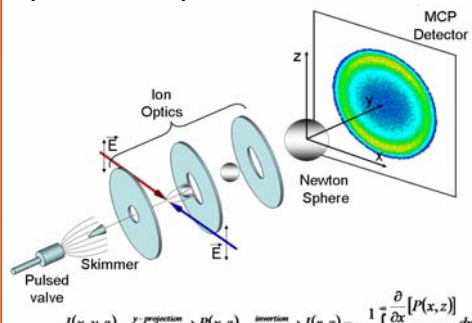


Introduction

Acetone plays an important role in the photochemistry of Earth's troposphere. Particular interest arises in the yield of acetyl (CH_3CO) radicals as a function of photolysis wavelength, because the reaction $\text{CH}_3\text{CO} + \text{O}_2$ has recently been identified as a new source for tropospheric OH [1].

Using velocity map imaging (VMI), we have monitored the CH_3 fragment from the photodissociation of acetone following S_1 - S_0 excitation at wavelengths between 333.5 and 230 nm. Our results provide clear evidence for three distinct photodissociation pathways.

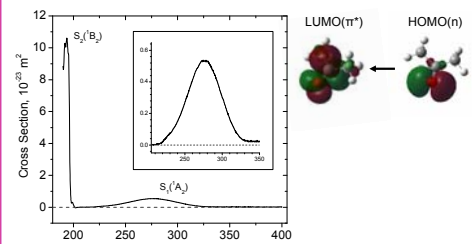
Experimental Setup



Characteristics of Acetone

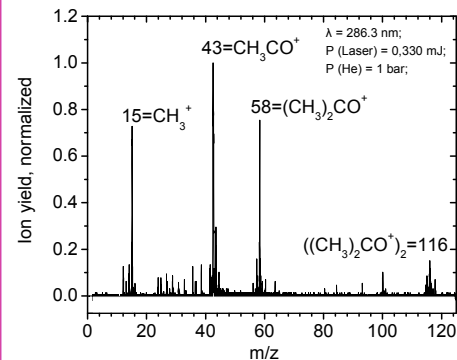
UV absorption spectrum of acetone

1st absorption band : $S_1(^1A_2) \leftarrow S_0(^1A_1)$ $\nu_0 = 30431 \text{ cm}^{-1}$



The UV absorption spectrum of gaseous acetone was recorded at a vapour pressure of 18 mbar and sample temperature of 23°C. The inset shows an enlarged view of the first absorption band used to investigate the dissociation dynamics of acetone.

Time-of-flight mass spectrum of acetone



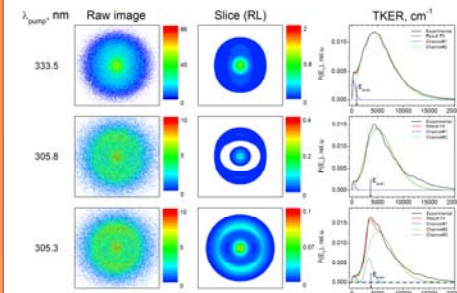
The TOF mass spectrum shows the ion signals due to the parent molecule ($(\text{CH}_3)_2\text{CO} = 58 \text{ amu}$) and photolysis reaction intermediates, corresponding to the acetyl ($\text{CH}_3\text{CO} = 43 \text{ amu}$) and methyl ($\text{CH}_3 = 15 \text{ amu}$) radicals. Unfortunately, it also exhibits an unwanted mass peak of (acetone), clusters which were hard to eliminate. Clusters of the higher orders were not detected.

Results

Velocity map images of acetone photolysis

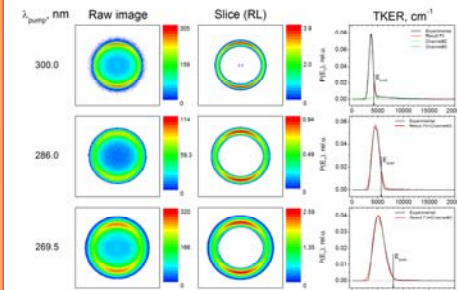
The photodissociation dynamics of the acetone molecule was investigated by observing the methyl photofragment spatial distribution as a function of photolysis wavelength. The formed methyl radical was probed in its ground vibrational state ($\nu = 0$) by (2+1) REMPI scheme resonantly exciting the Q-branch (all J) of the $3p^2A_2$ Rydberg state at 333.5 nm.

1. VMIs at 333.5 nm > $\lambda_{\text{photolysis}} > 305.3 \text{ nm}$



A ring-like feature (channel #3) in the observed methyl fragment distribution just appeared when the excitation energy exceeds the value of $2285 \pm 40 \text{ cm}^{-1}$ above the origin of the S_1 - S_0 transition (30431 cm^{-1} [2]). The off-set in the corresponding total kinetic energy distribution (TKER) profile points at the presence of the dissociation barrier on the potential energy surface.

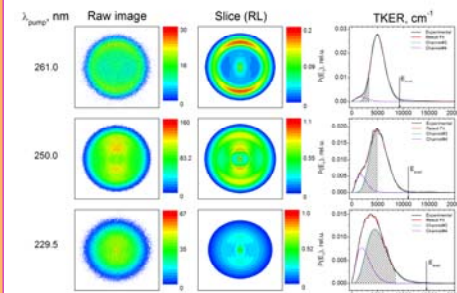
2. VMIs at 305.3 nm > $\lambda_{\text{photolysis}} > 261 \text{ nm}$



Increasing the excitation energy eliminates all other channels on the TKER profiles but channel #3. Further shortening of the photolysis wavelength shifts the peak position to the region of higher energy and the distribution gets broader.

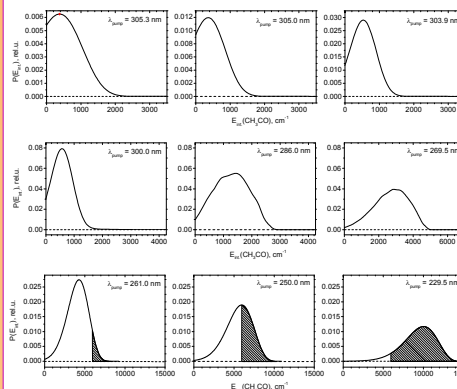
Dissociation energy was determined to be equal to: $D_0 = 29\,090 \pm 300 \text{ cm}^{-1}$

3. VMIs at 261 nm > $\lambda_{\text{photolysis}} > 229 \text{ nm}$

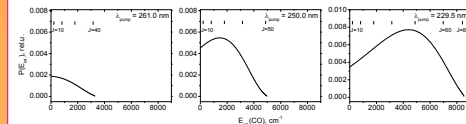


The TKER distributions gain a bimodal shape at excitation wavelengths shorter than 261 nm. The hatched area represents the fraction of acetyl fragments possessing enough internal energy to undergo secondary dissociation. This upper limit for the internal energy was calculated from the approximation that $E_{\text{int}}(\text{CH}_3) = 0 \text{ cm}^{-1}$ and the known dissociation energy of the acetyl molecule of $D_0 = 5945 \text{ cm}^{-1}$ [3].

Internal energy distributions of the acetyl photofragment



Internal energy distribution of CO photofragment



Vertical marks represent the rotational levels of CO calculated assuming a non-rigid rotator (rotational constant $B = 1.93 \text{ cm}^{-1}$, centrifugal distortion parameter $D = 6 \cdot 10^{-6} \text{ cm}^{-1}$).

High rotational excitation is caused by a strong torque, imparted to the CH_3CO fragment after the parent acetone molecule has decomposed and pushed acetyl out of the linear configuration resulting in high rotational energy of CO.

Table of energy distributions for the primary acetone and secondary acetyl dissociation (channels #3 and #4) and the angular anisotropy parameter β .

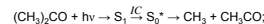
λ_{ph} , nm	E_{avail}	E_T	ΔE_T	$\langle E_T \rangle / \Delta E_T$	$\langle E_{\text{Acetyl}} \rangle$	Ch. #4, %	$E_{\text{CO}}^{\text{rot}}$	β
305.3	3667	3290	1620	0.89	378	—	—	0.23
300	4243	3669	915	0.86	574	—	—	0.20
286	5875	4552	1560	0.77	1434	—	—	0.20
269.5	8016	5030	2463	0.63	2862	—	—	0.18
261	9224	4940	3112	0.54	4284	6	0	0.21
250	10910	4966	3900	0.46	5944	40	1455	0.12
229.5	14483	4466	4690	0.31	10017	45	4392	0.11

All energies are given in cm^{-1} .

Discussion and Conclusion

Region 1 ($333.5 \text{ nm} < \lambda_{\text{photolysis}} < 305.3 \text{ nm}$):

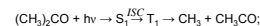
Acetone photolysis results in CH_3 fragments with low, narrow kinetic energy distributions formed via $S_1 \rightarrow S_0^*$ internal conversion and subsequent unimolecular decay on the S_0 potential energy surface (PES).



Such dissociation results in a statistical and isotropic distribution of fragments.

Region 2 ($305.3 \text{ nm} < \lambda_{\text{photolysis}} < 261 \text{ nm}$):

In this region, much faster CH_3 photofragments are produced by dissociation via the T_1 state. From the maximal translation energy release at the threshold wavelength of 305.3 nm, a dissociation barrier height on the T_1 PES of $4\,700 \pm 40 \text{ cm}^{-1}$ was obtained.



Region 3 ($229 \text{ nm} < \lambda_{\text{photolysis}} < 261 \text{ nm}$):

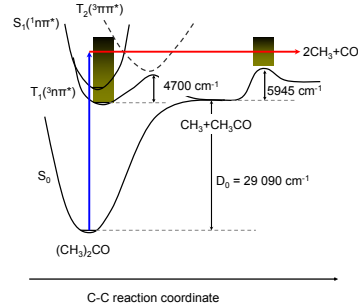
At $\lambda_{\text{photolysis}} < 261 \text{ nm}$, the excess energy is sufficient to allow for a secondary dissociation of the intermediate acetyl fragment, resulting in a bimodal CH_3 kinetic energy distribution.

Another possible explanation of the bimodal TKER profile is a conical intersection (CI) of the S_1 and S_0 PESs [4]. Such dissociation mechanism would not produce CO fragments which actually were observed in acetone dissociation at 248 nm [3,5]. Also, the CI can result in both α -CC bond cleavage and population of high vibrational levels of the S_0 PES, but no photon absorption from the high vibration levels was detected.

The isotropic photofragment distributions observed in these experiments suggest that IVR and rotation occur prior to dissociation.

The results provide information on the internal energy distribution in the CH_3CO fragment, which dictates the unimolecular decay rate of the CH_3CO in the atmosphere in competition with the reaction with O_2 .

Finally, a $\text{CH}_3\text{CO}-\text{CH}_3$ bond dissociation energy of $D_0 = 29\,090 \pm 300 \text{ cm}^{-1}$ was determined.



Literature

[1] A. Maranzana, J. R. Barker and G. Tonacchini, *PCCP*, **2007** (9), 4129.
 [2] Y. Haas, *Photochem. Photobiol. Sci.*, **2004** (3), 6.
 [3] H. Somnitz, M. Frida, T. Ufer and R. Zeltner, *PCCP*, **2005** (7), 3342.
 [4] E. W.-G. Diau, C. Koetting and A. H. Zewail, *CHEMISTRY*, **2001** (2), 273.
 [5] S.W. North, D. A. Blank, J. D. Gezelter and C. A. Longfellow, *J. Chem. Phys.*, **1995** (11), 4447.